A platinum butterfly effect: small changes turn an anticancer drug into a non-toxic metalloantibiotic with in vivo efficacy

npj | antimicrobials & resistance

Article

https://doi.org/10.1038/s44259-026-00211-w

A platinum butterfly effect: small changes turn an anticancer drug into a non-toxic metalloantibiotic with in vivo efficacy

Çağrı Özsan[1,2,7], Ann-Britt Schäfer[3,4,7], Abdul Akhir[5], Obed Akwasi Aning[3,4], Sofia Fulgencio[1], Rahul Maitra[5], Rupa Rani[3,4], Deepanshi Saxena[5], Fredrik Westerlund[3,4], Sidharth Chopra[5,6], Michaela Wenzel[3,4] ✉ & Angelo Frei[1,2] ✉

Metal-based compounds have emerged as a promising class of potential antibiotics exhibiting high hit-rates against critical bacterial pathogens while not displaying higher toxicity than organic compounds. Here, we describe the exploration of novel, non-toxic, Gram-positive acting platinum-based antibacterial agents with high activity. Structure-activity relationship (SAR) studies revealed that the simplest scaffold showed the best antibacterial properties. Mode of action studies showed that lead compound **Pt1** akin to the structurally similar chemotherapeutic cisplatin, causes reduced DNA staining, visible nucleoid compaction, and activation of DNA damage repair responses. Importantly, we show that **Pt1** interacts with and damages DNA directly, resulting in DNA strand breaks and fragmentation. **Pt1** activity can be reduced by hydroxyl radical scavengers, suggesting that **Pt1** possesses a multimodal mechanism. In line with this observation, no resistance development to **Pt1** was observed. Finally, we demonstrate the in vivo activity of **Pt1**, which significantly reduced the bacterial load in a murine *S. aureus* skin infection model. These findings shed light on the SAR and antibacterial mode of action of a novel class of platinum metalloantibiotics, validate their in vivo efficacy, and pave the way for further exploration of platinum compounds as novel antibiotic drug candidates.

Antimicrobial resistance (AMR) has emerged as one of the most significant health problems of the 21st century[1]. In 2019, 4.95 million deaths were associated with bacterial AMR, and it was the direct cause of 1.27 million of those. It is forecasted to be the leading cause of mortality by 2050, with approximately 10 million annual deaths[2]. At the same time, the conventional pipeline for antibacterial drug development, relying on organic medicinal chemistry, shows insufficient development to avert this scenario. Between 2013 and 2022, only 19 new small-molecule antibacterial drugs were approved, none of which introduced a first-in-class mechanism of action[3]. Since 2019, only three small-molecule antibiotics, Lefamulin, gepotidacin, and zoliflodacin have been approved with novel mechanisms, representing the first new classes since the approval of the tuberculosis drug bedaquiline in 2012[3–6]. This stagnation emphasizes a need to explore novel chemical spaces and unconventional approaches in antibacterial drug discovery.

Most antibiotics do not conform to the traditionally established medicinal chemistry structural criteria such as Lipinski's Rule of Five[3,7]. It is hence highly likely that entire classes of antibiotics remain unexplored due to having been excluded from screening campaigns based on inadequate criteria. To investigate previously unexplored chemical spaces, the Community for Open Antimicrobial Drug Discovery (CO-ADD) was launched in 2015. Compounds submitted to CO-ADD are evaluated against key bacterial and fungal pathogens to identify novel antimicrobial scaffolds[8]. A considerable amount of the submitted compounds do not meet the 'usual drug-likeness' properties including a notable class: metal complexes. Among 906 submitted metal complexes, representing 29 different metals, 246 demonstrated activity against bacterial strains, a remarkable hit rate of 27%, especially considering that purely organic molecules only showed a hit rate of 1.6%. Moreover, 9.9% of the metal complexes exhibited antibacterial

[1]Department of Chemistry, Biochemistry & Pharmaceutical Sciences, University of Bern, Bern, Switzerland. [2]Department of Chemistry, University of York, York, UK. [3]Division of Molecular Bioscience, Department of Life Sciences, Chalmers University of Technology, Gothenburg, Sweden. [4]Center for Antibiotic Resistance Research in Gothenburg (CARe), Gothenburg, Sweden. [5]Department of Molecular Microbiology and Immunology, CSIR-Central Drug Research Institute, Lucknow, India. [6]Academy of Scientific and Innovative Research (AcSIR), Ghaziabad, India. [7]These authors contributed equally: Çağrı Özsan, Ann-Britt Schäfer. ✉e-mail: wenzelm@chalmers.se; angelo.frei@york.ac.uk

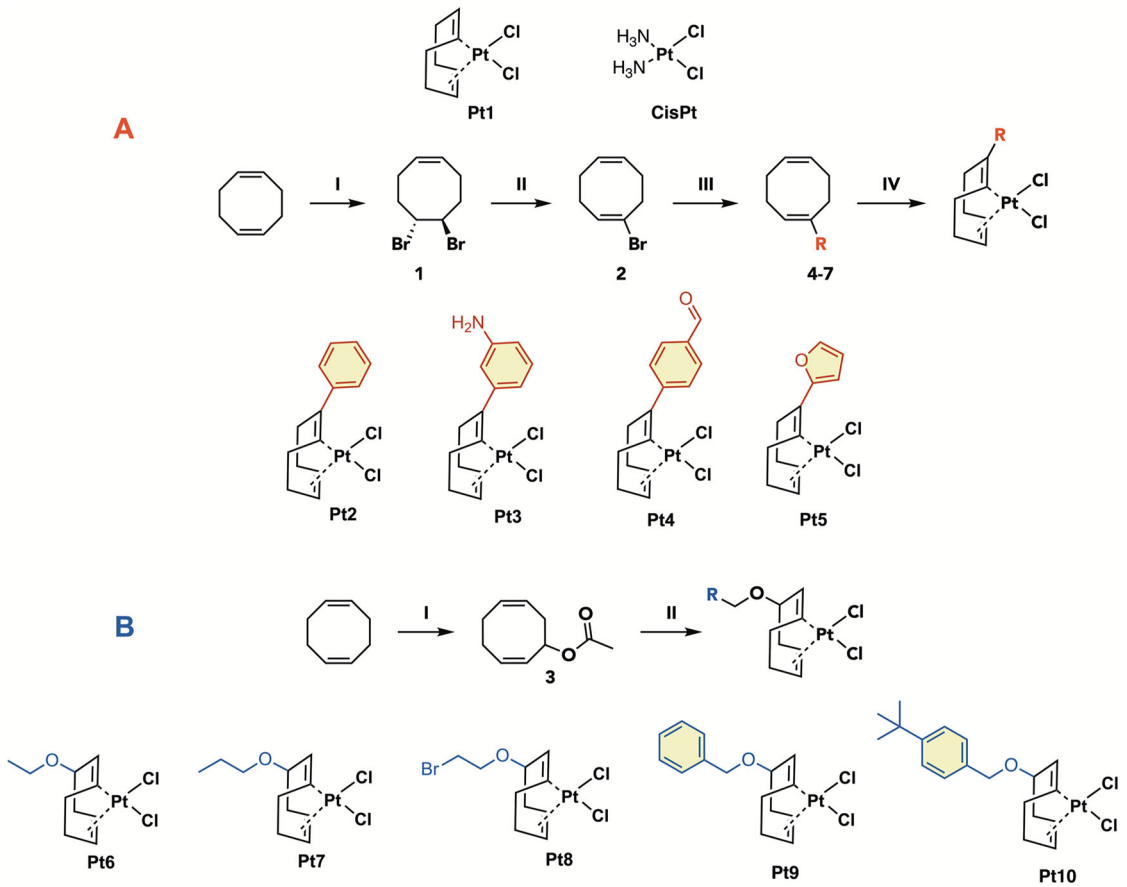

Fig. 1 | Reaction scheme for double bond-modified COD ligands and corresponding Pt(II) complexes. A I: Br_2, DCM, 30 min, r.t., 77%; **II:** DBU, DMF, overnight, 80 °C, 21%; **III:** $RB(OH)_2$, $Pd(PPh_3)_4$, Na_2CO_3, Dioxane:H_2O, 4 h, reflux, 28–41%; **IV:**K_2PtCl_4, EtOH:H_2O, 1 h, MW, 90 °C, 12–55%. **B** Reaction scheme for allylic position modified Pt(II) complexes. **I:** *t*-butylhydroperoxide, CuCl, AcOH, 52 h, reflux, 7%; **II:** K_2PtCl_4, H_2O:RCH_2OH, 1 h, MW, 90 °C, 7–13%.

activity without significant cytotoxicity to human cells, over ten times the rate observed in the general CO-ADD library (0.87%) [9].

Metal complexes could be the key to the 'escape from flatland' of purely organic molecules with their highly three-dimensional structures offering greater structural diversity[10,11]. Morrison et al. demonstrated that a library of 71 selected 'metallofragments' exhibits significantly greater three-dimensionality compared to a library of over 18,000 organic small molecules[12]. As molecular interactions with biological systems are fundamentally structure-dependent, molecular shape represents a critical factor in determining biological activity. Consequently, broad structural diversity is a highly desirable property to maximize the likelihood of identifying hits against diverse biological targets[12–15]. In addition to the geometrical diversity, metal complexes can offer unique modes of action such as ligand exchange or release, redox properties, catalytic characteristics to form toxic species, and exchange of metals that stabilize the native structures of proteins causing malfunction and denaturation [9,11,16–18].

The exploration of inorganic or metal-based compounds as medicines is not a novel area of research. Indeed, many inorganic compounds are used in the clinics today and many more are under clinical investigation[19]. The golden age of inorganic medicinal chemistry started with the approval of the first platinum-based chemotherapy agent, cisplatin (**CisPt**), in 1978. Today, platinum-drugs are still used as a gold-standard first-line chemotherapy against many cancer types[20,21]. In the aforementioned CO-ADD study, platinum complexes represented the highest number of active metal-based compounds with low cytotoxicity[9]. Interestingly, the antibacterial potential of platinum complexes had already been noticed by Rosenberg and colleagues as an unexpected result of an electrochemical experiment with *Escherichia coli*[22,23]. Until Lippard and co-workers reported monofunctional platinum complexes as inducers of bacterial filamentation and lysis in lysogenic *E. coli* in 2014, there had been no investigation of platinum complexes as antibacterial agents as the focus shifted to cancer research[24]. In recent years, there have been more studies on the antimicrobial properties of platinum complexes [25–31].

In 2021, Frei et al. established 1,5-cyclooctadiene (COD) platinum complexes (PtCOD) as promising antibacterials against Gram-positive bacteria. Structure-activity relationship (SAR) studies of this compound class revealed that PtCOD complexes bearing two halogen ligands (**Pt1**, Fig. 1) maintain promising activity against a broad panel of Gram-positive bacteria. Additionally, in vivo toxicity was evaluated using larvae of the greater wax moth *Galleria mellonella*, and no toxicity was observed up to 0.4 mM (6–7.5 mg/kg) [32].

Overall, PtCOD complexes have shown promising antibacterial activity with no in vitro or in vivo toxicity. To further explore the potential of PtCOD compounds as metalloantibiotics, we embarked on an exploration of their structure-activity relationships and antibacterial mechanisms. Herein, we report a detailed study of the biological profile of this compound class. By preparing a series of new derivatives and conducting a range of mechanistic studies we elucidate the mechanism of action of **Pt1**, evaluate its propensity to induce resistance, and assess its in vivo efficacy in a murine skin infection model.

Results

Synthesis of Pt(COD-R)Cl_2 Complexes

In previous work[32], PtCOD complexes bearing halogen ligands have been investigated and found as promising antibacterial agents against Gram-positive bacteria with, **Pt1** becoming a new lead compound[32]. To further elucidate their SAR, novel derivatives of this compound class were synthesized. Given the observed significance of the halogen ligands in

conferring antibacterial activity, we aimed to explore modifications on the COD ring. The modifications were performed either at the double-bond (Fig. 1A, **Pt2-5**) or allylic position (Fig. 1B, **Pt6-Pt10**) starting from commercially available COD. The modified ligands were reacted with K_2PtCl_4 to obtain the final complexes. All final complexes were purified by silica chromatography and characterized by NMR and Mass Spectrometry (cf. Supporting Information).

Antibacterial activity of Pt(COD-R)Cl_2 complexes

To assess the antibacterial activity of the complexes, minimum inhibitory concentration (MIC) assays were conducted against representative Gram-positive bacteria, namely methicillin-sensitive *Staphylococcus aureus* (MSSA), methicillin-resistant *S. aureus* (MRSA), and *Bacillus subtilis* (Table 1A). Substituting the double bond with benzyl or furan rings (**Pt2-5**) significantly reduced activity against Gram-positive strains. While **Pt2** showed limited activity (MIC 50–100 µM), the other complexes were inactive in this concentration range. In contrast, modifications at the allylic position demonstrated good antibacterial activity (**Pt8**), yet did not exceed the activity of the parent compound **Pt1**.

None of the complexes showed antibacterial activity against *E. coli* (Table S1). The structural similarity between the platinum-based anticancer drug **CisPt** and our lead compounds led us to examine the antibacterial effects of the anticancer drugs **CisPt** and oxaliplatin against Gram-positive bacteria, yet neither showed activity up to 100 µM (Table 1A and S2). The antibacterial activity of **CisPt** has been investigated several times since the first report by Rosenberg et al. However generally only moderate levels of activity were observed and generally this was lower against Gram-positive strains compared to Gram-negative strains [33,34].

To confirm whether the observed antibacterial activity originates from the complexes themselves, rather than the ligand (COD) or platinum alone, the antibacterial effects of 1,5-cyclooctadiene and K_2PtCl_4 against *S. aureus* and *E. coli* were examined. Neither of them were found to be active up to 200 µM (Table S3).

The parent compound **Pt1** as well as **Pt8**, which was the most promising amongst the newly synthesized allylic-modified complexes, were selected as lead compounds for further characterization. To this end, their antibacterial activity against an extended Gram-positive panel including a range of MRSA and vancomycin-resistant *S. aureus* (VRSA) strains was assessed (Table 1B, see Table S5 for corresponding values in µg/mL). **Pt1** showed excellent activity against the whole panel, while **Pt8** was slightly less active. Both lead compounds were also tested against an extended Gram-negative panel consisting of *E. coli*, *Klebsiella pneumoniae*, *Acinetobacter baumannii*, and *Pseudomonas aeruginosa*. However, neither compound was active up to the highest tested concentrations (Table S5). The addition of sublethal concentrations of outer membrane permeabilising polymyxin B nonapeptide (PMBN)[35] did not enhance the activity of **Pt1** against *E.coli*, (Table S4) and no antibacterial effect was observed up to the highest concentration tested. Furthermore, our previous study[32] demonstrated that **Pt1** was inactive against *E. coli* tolC and *E. coli* lpxC mutant strains, which are impaired in efflux and lipid A biosynthesis, respectively. In combination with the absence of activity in the presence of PMBN, these findings indicate that outer membrane permeability and efflux are not the primary factors

Table 1 | Antibacterial activity and cytotoxicity

A. Antibacterial Activity of PtCOD Library

Strain		Pt1	Pt2	Pt3	Pt4	Pt5	Pt6	Pt7	Pt8	Pt9	Pt10	CisPt	Van
MSSA	Clin. Is.	3.13–6.25	50–100	>100	>100	>100	12.5	>100	12.5	12.5–25	12.5–25	>100	0.86
MRSA	COL	3.125	100	>100	>100	>100	12.5	12.5	12.5–25	6.25	12.5	>100	0.86
Bs	MW168	6.25	100	>100	>100	>100	100	50–100	50	50–100	25	>100	<0.22

B. Gram-positive Panel (Pt1 & Pt8)

Strain		MIC [µM]		
		Pt1	Pt8	Van
MSSA	**ATCC 29213**	0.67	4.02	0.67
MRSA	**NRS 100**	0.67–1.34	8.04–16.1	1.34
	NRS 119	0.33–0.67	2.01	1.34
	NRS 129	0.33–0.67	2.01–4.02	0.67
	NRS 186	0.33–0.67	4.02–16.1	0.67
	NRS 191	0.67	2.01–4.02	1.34
	NRS 192	0.33–0.67	2.01	0.67-1.34
	NRS 193	0.67	4.02	1.34
	NRS 194	0.33–0.67	2.01	0.67
	NRS 198	0.67	8.04	1.34
VRSA	**VRS 1**	0.67–1.34	64.3	>43.1
	VRS 4	0.67–1.34	8.04	>43.1
	VRS 12	0.67–1.34	8.04–16.1	>43.1

C. Toxicity Assays (Pt1 & Pt8)

Cell Line		Pt1	Pt8	CisPt
Vero	**72 h**	>134	>402	n.d.
HEK293T	**24 h**	74.1 ± 4.1	92.2 ± 3.9	81.6 ± 5.1
	48 h	65.3 ± 2.7	84.8 ± 10.1	22.04 ± 3.4
RBC		>200	>200	n.d.

(**A**) MICs (µM) of synthesized PtCOD complexes against a selection of Gram-positive strains. (**B**) MICs (µM) of lead compounds **Pt1** and **Pt8** against an extended panel of drug-resistant *S. aureus* strains. Vancomycin (Van) was used as positive control. (**C**) IC_{50} and HC_{50} values (µM) of **Pt1** and **Pt8** against mammalian cell lines and human red blood cells.
MSSA methicillin-susceptible *S. aureus*, *Clin. Is*. clinical isolate, *MRSA* methicillin-resistant *S. aureus*, *Bs Bacillus subtilis*, *VRSA* vancomycin resistant *S. aureus*, *RBC* human red blood cells.

limiting **Pt1** activity in Gram-negative bacteria. The difference in the activity difference between Gram-positive and Gram-negative bacteria could be due to limited transport of **Pt1** across the inner membrane, preventing the compound from reaching its intracellular target.

Hemolytic and cytotoxic activity of Pt(COD-R)Cl_2 complexes

Selectivity of antibacterial compounds for bacteria over mammalian cells is essential. Therefore, 50% hemolytic concentrations (HC_{50}) were determined against human red blood cells (RBC). All tested PtCOD complexes showed HC_{50} values above 200 μM and were thus classified as not hemolytic (Table 1C and S6).

To test cytotoxicity of the lead compounds against mammalian cell lines, 50% inhibitory concentrations (IC_{50}) were determined against African Green Monkey kidney cells (Vero) and Human embryonic kidney cells (HEK293T). In vitro kidney cell models are widely considered a gold-standard approach for nephrotoxicity screening in drug discovery as the kidneys are a primary target organ for chemical-induced injury and play a central role in drug excretion [36].

Neither **Pt1** nor **Pt8** significantly reduced the viability of Vero cells up to the highest tested concentrations (134 μM and 402 μM respectively, Table 1C and Fig. S3). IC_{50} values of **Pt1** (74.1 ± 4.1 μM) and **Pt8** (92.2 ± 3.9 μM) against HEK293T cells after 24 h were comparable to those of **CisPt** (81.6 ± 5.1 μM). However, neither **Pt1** (65.3 ± 2.7 μM) nor **Pt8** (84.8 ± 10.1 μM) showed a large increase of toxicity after 48 h, which is in stark contrast to **CisPt** (22.04 ± 3.4 μM, Table 1C and S7, Figs. S1–2).

Taken together, **Pt1** and **Pt8** show promising antibacterial activity against a broad panel of Gram-positive pathogens but do not cause hemolysis and exhibit only minor toxicity against mammalian cell lines at concentrations necessary to elicit antibacterial effects. However, as shown in our previous study[32]**Pt1** lost its antibacterial activity completely in human serum, indicating strong serum interactions and reduced systemic efficacy. Indeed, no in vivo activity was observed in a systematic infection model in *Galleria mellonella*. Therefore, this compound class may not be suitable for systemic (oral or intravenous) administration. Instead, these compounds appear more suitable for topical applications, where serum binding is less relevant (*vide infra*).

Mode of action studies of Pt1 and Pt8

Encouraged by these results, we proceeded to study the modes of action of **Pt1** and **Pt8** in comparison with **CisPt** using phenotypic analysis of the Gram-positive model organism *B. subtilis*. To this end, we first confirmed the MICs against *B. subtilis* 168CA, the background strain of our reporter constructs (**Pt1**: 6.25 μM; **Pt8**: 50 μM). Based on these values, we determined the optimal stressor concentrations (OSCs) in acute shock experiments. The optimal stressor concentration is a concentration that leads to a 50–70% reduction of bacterial growth during mid-exponential phase. It imposes sufficient stress to elicit a clear phenotype without causing excessive cell death or lysis, which would mask the direct effects of the test compound[29]. We determined OSCs of 3.125 μM for **Pt1** and 25 μM for **Pt8** (Fig. S4). No growth inhibition could be observed with **CisPt** (Fig. S4), leading to the decision to proceed with the highest tested concentration (100 μM). Both **Pt1** and **Pt8** showed a reproducible delay until the onset of growth inhibition (~30 min for **Pt1** and ~60 min for **Pt8**, Fig. S4). Hence, we chose 30 and 60 min after antibiotic addition as timepoints for phenotypic analysis experiments.

Bacterial cytological profiling

To get an overview of the cellular effects of the compounds, we employed bacterial cytological profiling (BCP). To this end, we used a strain intracellularly expressing green-fluorescent protein (GFP) from the strong, constitutive *PrpsD* promoter (*B. subtilis* bSS82[37]), stained with the membrane dye Nile red and the DNA dye DAPI. Combined with phase contrast microscopy, this setup allows simultaneous assessment of cell morphology, cell lysis, pore formation, membrane morphology, and nucleoid morphology in one assay [38].

None of the compounds caused apparent differences in overall cell morphology (phase contrast) or compromised membrane integrity (GFP) (Fig. 2A). Nile red foci, indicating membrane stress, were observed in **Pt1**-treated samples. However, quantification of the percentage of cells exhibiting Nile red foci could not statistically support this observation due to high variability among treated samples (Fig. S5). These results suggest that membrane damage may be a secondary component of the **Pt1** mode of action that may occur to varying degrees, but it is unlikely to be the primary mechanism of action.

Striking effects of **Pt1** and **Pt8** were observed on the bacterial nucleoid (DAPI), showing visible changes in both nucleoid morphology and fluorescence intensity (Fig. 2A). When we quantified these differences, both **Pt1** and **Pt8** as well as **CisPt** showed clear nucleoid compaction after 60 min of treatment (Fig. 2B). This is indicative of DNA packing defects. Similarly, **Pt1** and **CisPt** caused a significant reduction of the DAPI signal in the same timeframe, **Pt8** showing a similar trend. This phenotype points towards compromised DNA integrity and can indicate DNA fragmentation or other structural changes that decrease the availability of the minor groove to the DAPI dye (Fig. 2C). These results gave rise to the hypothesis that **Pt1** and **Pt8** affect the structural integrity of DNA, and consequently nucleoid packing, possibly in a manner similar to **CisPt**.

DNA damage

BCP revealed that **Pt1** and **Pt8** elicited their strongest effect on the bacterial nucleoid, both in terms of nucleoid packing and fluorescence intensity of the DAPI stain (Fig. 2). A reduced DAPI signal indicates less efficient DNA binding of the dye, suggesting inaccessibility of the minor groove[39] and thus structural changes to the DNA. To confirm whether the compounds induce DNA damage in bacterial cells, the localization of RecA was assessed. RecA is part of the bacterial SOS response to DNA damage. It is a DNA-associated protein that recognizes single-stranded DNA, which occurs as a consequence of strand breaks. If strand breaks are present, RecA accumulates at the damaged sites, appearing as foci or elongated structures[40]. Since the RecA response is strongest shortly after stress induction[41], we additionally examined a 10 min timepoint in this assay. Indeed, clear RecA accumulations were found on the nucleoids of cells treated with **Pt1, Pt8**, and **CisPt**, with the strongest response induced after 10 min and **Pt1** showing the most pronounced effects (Fig. 3).

We then wondered whether the compounds directly interact with and damage DNA. To address this, commercially available λ-phage DNA (λ-DNA) was incubated with **Pt1, Pt8**, and **CisPt**, followed by staining with the DNA dye YOYO-1 and stretching of DNA strands on functionalized glass slides. Samples were then subjected to single-molecule fluorescence imaging followed by length analysis of individual DNA strands[42]. We observed a clear shift of the DNA molecule length, revealing shorter fragments in samples treated with 3.125 μM **Pt1**, 25 μM **Pt8**, and 100 μM **CisPt** (Fig. 4). These findings demonstrate that the compounds do indeed directly interact with and damage DNA. The data further shows that both **Pt1** and **Pt8** induce strand breaks, which was expected based on the RecA recruitment results (Fig. 3). These observations match the known mechanism of **CisPt**, which causes 1,2-intrastrand cross-links of purine bases leading to single strand DNA breaks[43]. Taken together, these results confirm DNA damage as the primary mechanism of **Pt1** and **Pt8**.

Interestingly, **Pt1**, which was the most potent antibacterial agent, had the mildest effects on λ-DNA. We wondered whether this observation may be due to the different concentrations, which were based on the OSC determined for *B. subtilis* cultures. Therefore, we additionally tested 25 μM **Pt1** and 3.125 μM **Pt8** to directly compare equimolar concentrations. While an increase of **Pt1** clearly showed stronger DNA fragmentation, the decrease of **Pt8** did not diminish its effect (Fig. 4). These results suggest that **Pt8** is a more potent DNA-damaging agent.

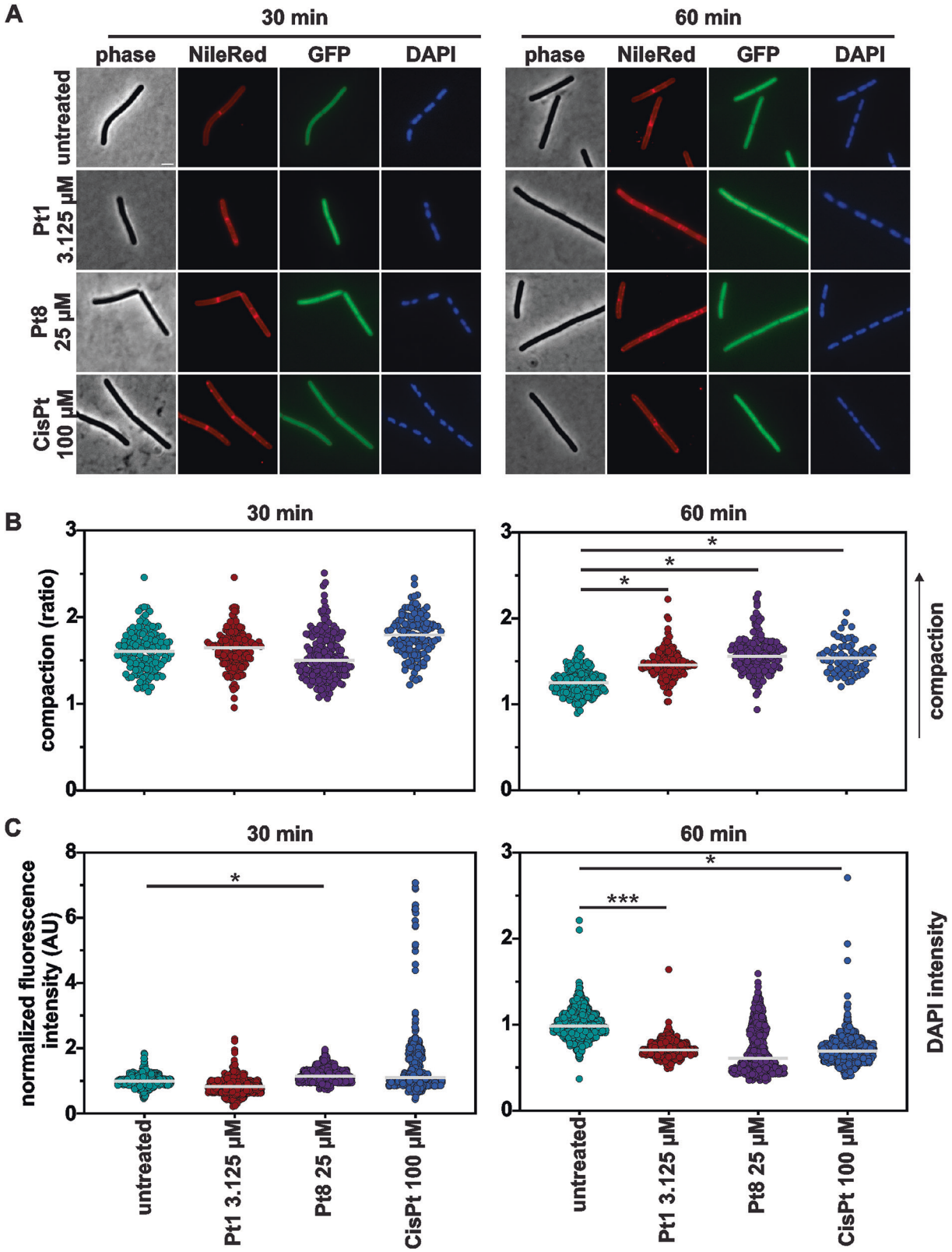

Fig. 2 | Bacterial cytological profiling of *B. subtilis* bSS82, constitutively expressing GFP from the *PrpsD* promoter, stained with Nile red (membrane) and DAPI (DNA). Cultures were treated with **Pt1** (3.125 µM), **Pt8** (25 µM), and **CisPt** (100 µM) for 30 and 60 min, respectively. **A** Phase contrast and fluorescence microscopy images. Scale bar 2 µm. Quantification of nucleoid compaction measured as a ratio of the whole cell area vs the area occupied by the DAPI-stained nucleoid (**B**) and DAPI fluorescence intensity (**C**). Gray lines indicate the median. Graphs show pooled data from three biological replicates. See Fig. S6 for cell populations divided by individual replicates. Significance was tested with nested t-tests (p values: *≤ 0.5, **≤ 0.01, ***≤ 0.001).

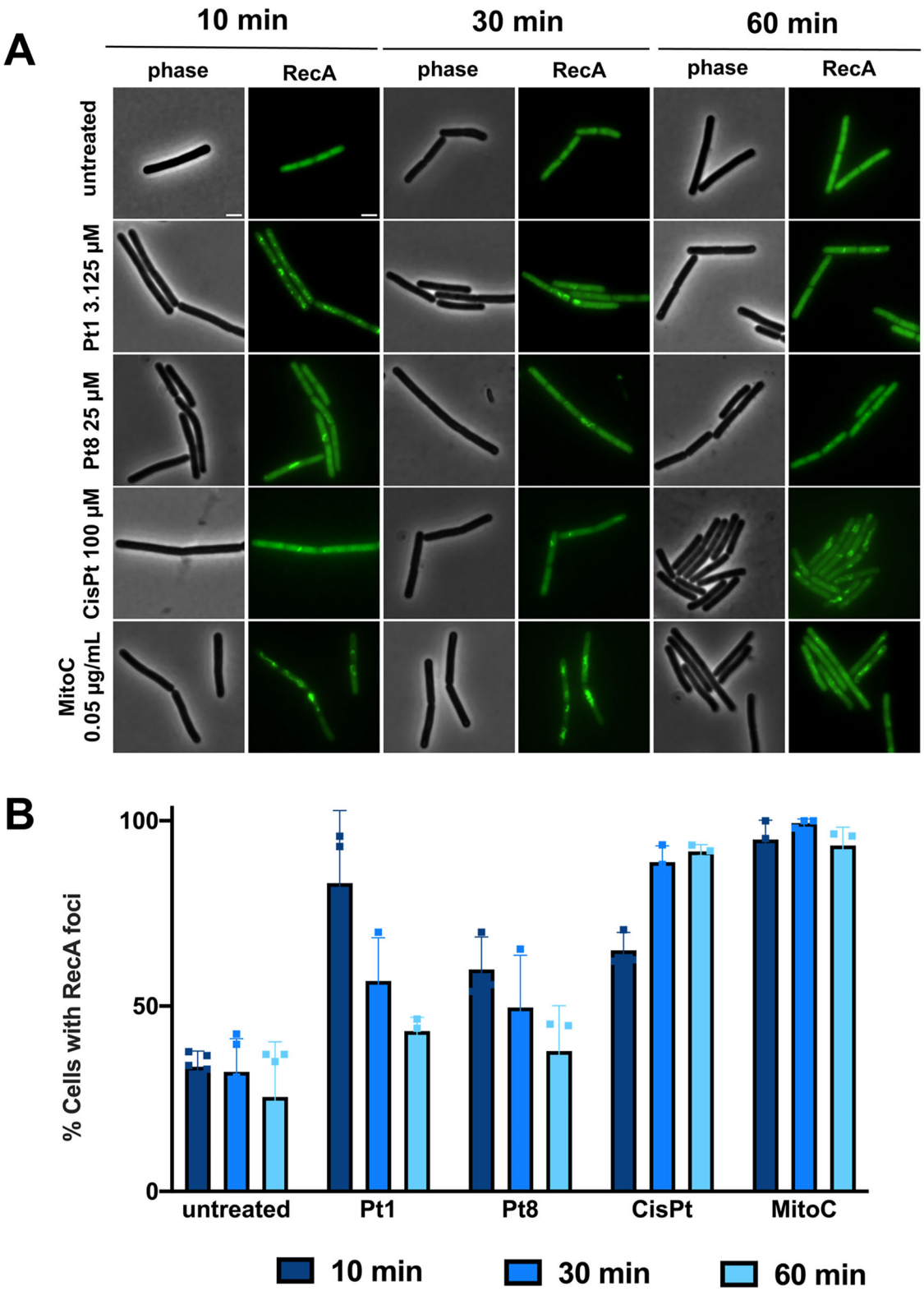

Fig. 3 | Localization of RecA-GFP (*B. subtilis* UG10) after treatment with Pt1 (3.125 µM), Pt8 (25 µM), and CisPt (100 µM). Mitomycin C (**MitoC**, 0.05 µg/mL) was used as positive control. **A** Phase contrast and fluorescence microscopy images. Scale bar 2 µm. **B** Quantification of microscopy images. Cells with distinct RecA foci were counted and expressed relative to the number of total cells. A minimum of 50 cells were counted per condition per replicate. Error bars show standard deviation of at least three biological replicates.

Cell envelope stress

Nile red stains suggested that **Pt1** could additionally partially act through membrane activity. We followed up on this lead to explore whether it may allow molecules smaller than GFP to pass the cell membrane[38]. We first tested the uptake of the membrane-impermeable, red-fluorescent dye propidium iodide (PI). Neither **Pt1** nor **Pt8** showed increased PI uptake confirming that they do not compromise membrane integrity (Fig. 5A). Nisin was selected as a positive control for this assay because of its well-

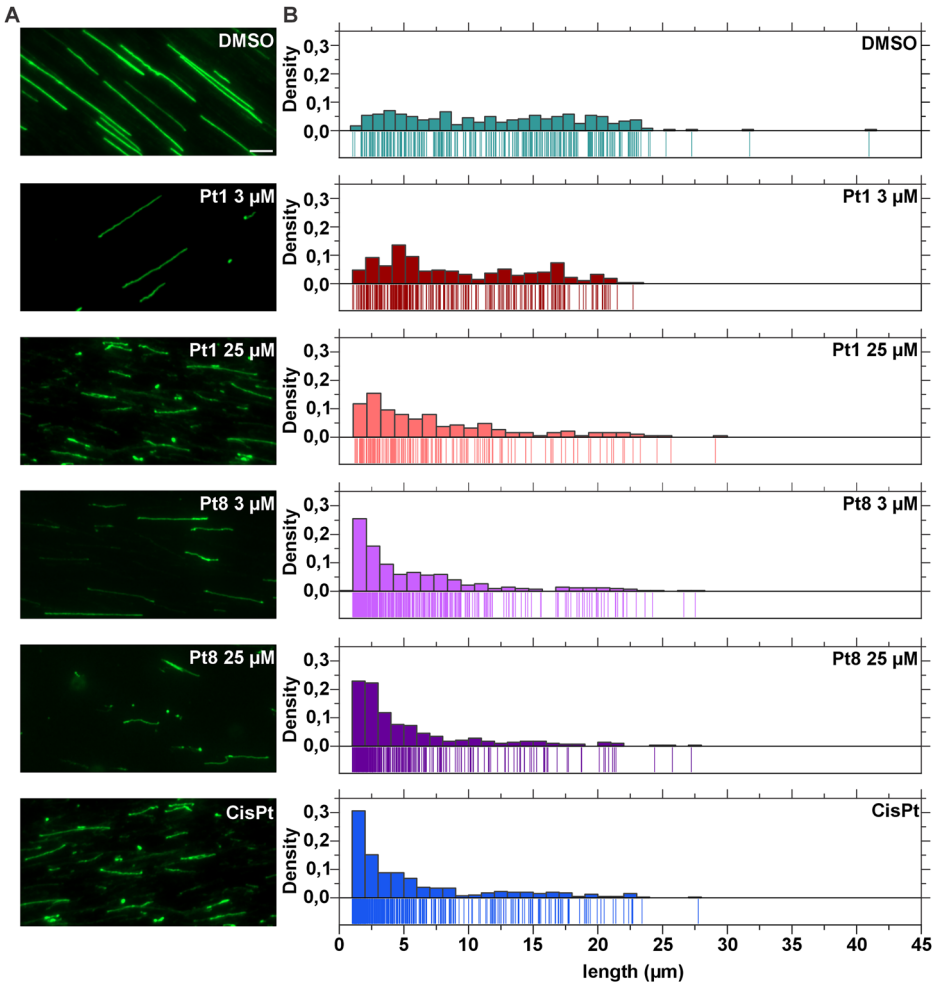

Fig. 4 | Single-molecule imaging of YOYO-1-labeled λ-DNA. A Fluorescence microscopy images of λ phage DNA exposed to the different lead compounds. DMSO was included as negative control. Scale bar 5 µm. **B** DNA strand length distribution measured from microscopy images (pooled from three biological replicates).

established pore-forming mechanism of action[38,44]. Likewise, no membrane depolarization could be observed when measured with the membrane potentiometric fluorescent dye 3,3'-dipropylthiadicarbocyanine iodide (DiSC(3)5)[45] (Fig. 5B), showing that no relevant ion translocation is caused by the compounds. Gramicidin is an ion pore that leads to rapid dissipation of the membrane potential and serves as standard positive control in membrane depolarization assays[45,46]. This finding was independently confirmed by assessing the localization of the cell division regulation protein MinD, which localizes at midcell and cell poles in healthy cells, but delocalizes into membrane-associated clusters upon loss of membrane potential[47] (Fig. 5C). These results show that neither **Pt1** nor **Pt8** affect membrane integrity.

Despite not being statistically significant, the tendency of **Pt1** and **Pt8** to cause membrane foci was apparent (Fig. S5). In addition to direct membrane damage, an impairment of cell wall synthesis or cell division can also cause Nile red foci[38,48]. To assess possible effects on these processes, we examined the localization of the proteins MreB and FtsZ. MreB is an actin homolog that moves around the lateral cell axis driving the cell wall elongation machinery forward. This movement stops when cell wall synthesis is impaired, making MreB mobility a reliable reporter for cell wall synthesis inhibition[38,49,50]. However, neither **Pt1** nor **Pt8** affected MreB mobility, showing that they do not inhibit this process (Fig. S7). Likewise, the localization of the tubulin homolog FtsZ, the major cell division protein in bacteria[51], remained unaffected demonstrating that the division machinery is not disturbed (Fig. S8). These results suggest that **Pt1** and **Pt8** do not elicit their antibacterial activity through impairment of cell envelope function.

Effects on transcription and translation

Strong GFP signal in the BCP suggested that the platinum compounds did not interfere with protein expression. However, *PrpsD* is a strong, constitutive promoter and mild effects will not be visible against the background of already accumulated GFP. To confirm that **Pt1** and **Pt8** do not affect the transcription and translation machineries, we assessed the localization of the RNA polymerase β' subunit RpoC and the ribosomal protein RpsB, which have been used as reporters for transcription and translation inhibition, respectively[52]. Neither protein showed a distinct phenotype after treatment with **Pt1** and **Pt8**, confirming our notion (Fig. S9–10).

We then directly tested their capacity to impair protein production using inducible GFP-MinD as readout. To this end, we added the respective compounds prior to induction of protein expression with xylose. No differences in GFP-MinD expression were observed, demonstrating that protein expression is unaffected by **Pt1** and **Pt8** (Fig. S11).

Compound uptake

Following the previous observations, we hypothesized that the difference in antibacterial activity between **Pt1** and **Pt8** may be due to less efficient uptake of the latter compared to the former, and that this is likely the reason underlying the poor antibacterial activity of **CisPt** as well. Therefore, we used inductively-coupled plasma mass spectrometry (ICP-MS) to assess compound uptake into MRSA based on detection of cellular Pt levels[53]. Indeed, **Pt1** showed much more efficient uptake than **Pt8**, while **CisPt** showed the lowest uptake (Figs. 6A and S12). Although the uptake percentages differ drastically between the lead compounds and **CisPt**, the absolute amounts of platinum in bacteria after treatment (**Pt1**: 3.5 µg/L, **Pt8**: 4.0 µg/L, **CisPt**: 2.6 µg/L) did not show a marked difference. While the

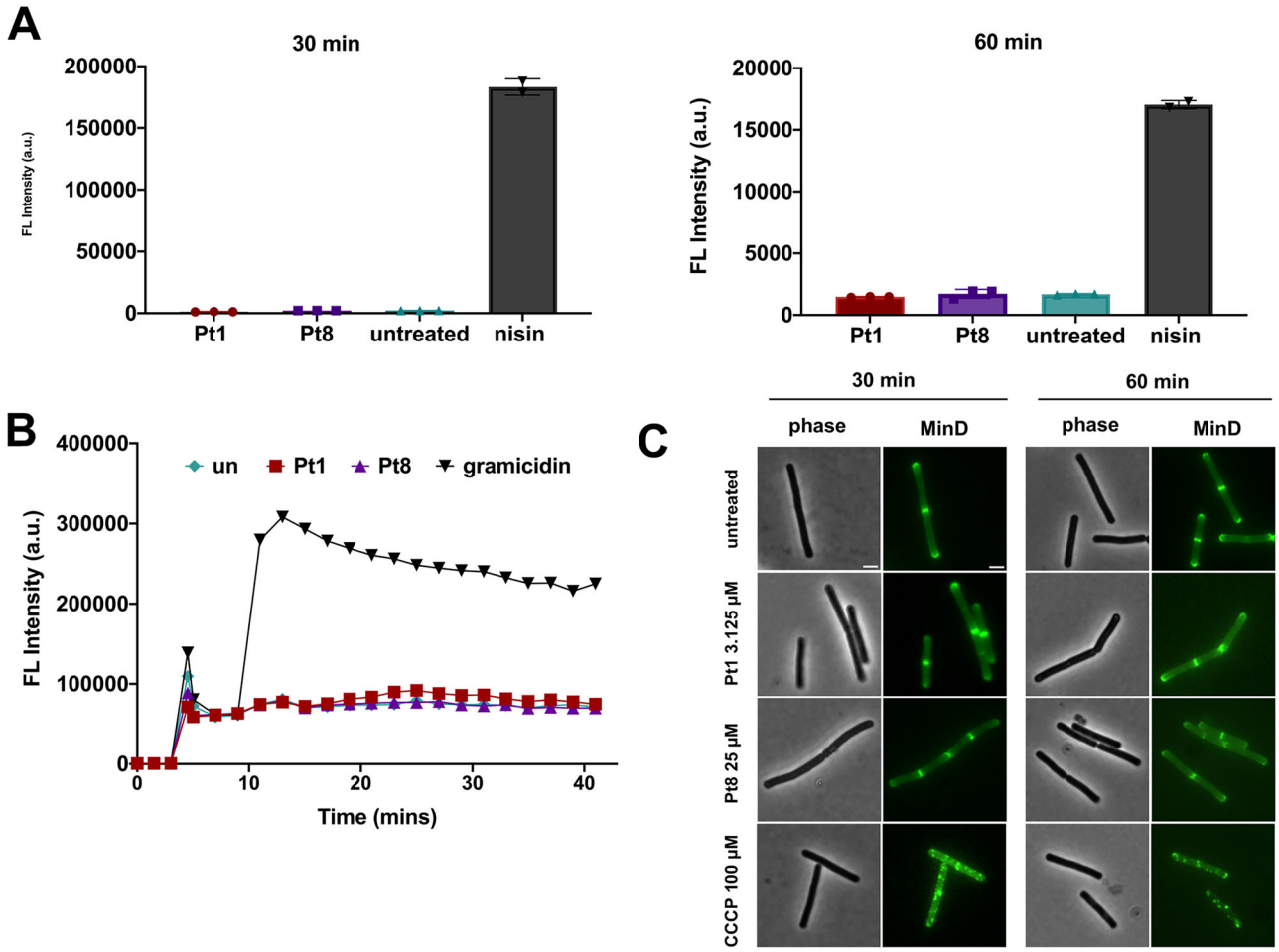

Fig. 5 | Effects on membrane integrity. A Propidium iodide staining of *B. subtilis* 168CA (pore formation assay). 0.23 µM nisin was used as positive control. Note the different scales at 30 and 60 min. **B** $DiSC_3(5)$) assay in *B. subtilis* 168CA (membrane depolarization assay). 0.53 µM gramicidin was used as positive control. **C** Localization of MinD-GFP in *B. subtilis* TB35 (*Pxyl-gfp-minD*). Localization of MinD depends on the membrane potential. 100 µM CCCP were used as positive control. All assays were performed after treatment with 3.125 µM **Pt1** and 25 µM **Pt8**. Scale bar 2 µm.

variation in uptake clearly plays an important role in the differences in antibacterial activity, other molecular factors likely contribute as well.

Reactive oxygen species

Metal complexes often induce oxidative stress in cells, which can significantly contribute to DNA damage, mostly through generation of hydroxyl radicals. While platinum cannot substitute for iron or copper in a Fenton reaction to create hydroxyl radicals from hydrogen peroxide, it has been shown to increase hydroxyl radical-mediated DNA damage[54] in a system capable of the Fenton reaction. Bacterial cells contain significant amounts of iron, and the Fenton reaction is a common source of hydroxyl radicals[55]. Exacerbation of DNA-damaging reactive oxygen species (ROS) in addition to direct DNA-damaging action constitutes a mechanism that could explain the higher antibacterial activity of **Pt1** compared to **Pt8**, in addition to more efficient uptake. To test whether ROS play a role in the activity of the compounds, a scavenger assay was employed. In this modified MIC assay, the activity of a test compound is determined in scavenger-free medium, medium containing the superoxide scavenger tiron, the hydroxyl radical scavenger thiourea, or a mix of both[41,56]. If ROS contribute to antibacterial activity, an increase of the MIC value is expected in medium containing the scavenger specific to the ROS that is generated. Thus, the antibacterial activity of hydrogen peroxide, a hydroxyl radical donor, was not significantly affected by the superoxide scavenger tiron, but in presence of the hydroxyl radical scavenger thiourea, the MIC increased by a factor of 14, and no additive effect was observed when tiron and thiourea were combined (Fig. 6B). The same trend was observed with **Pt1**, which showed a threefold MIC increase in medium containing tiron, a tenfold increase in the presence of thiourea, and a 13-fold increase in medium containing both scavengers. These results suggest that mostly hydroxyl radicals and to a lesser extent superoxide contribute to the activity of **Pt1**. Importantly, **Pt8** showed no notable MIC increase in the presence of ROS scavengers, confirming our notion that the increased activity of **Pt1** is due to the generation of ROS in addition to direct DNA damage. This finding could also explain the tendency of **Pt1** to induce Nile red foci, since ROS can also damage membrane lipids[57], likely contributing to the potency of the compound (Fig. 6C).

Advanced biological evaluation of Pt1

Amongst all evaluated PtCOD derivatives, **Pt1** displayed the best properties. It showed nano to low micromolar antibacterial activity across a panel of Gram-positive bacteria, displayed low toxicity, both in cell lines and in live *G. mellonella*[32], and possesses a new mode of action. Furthermore, **Pt1** reduced the fungal load in a *G. mellonella* model of *C. albicans* infection in previous studies[31]. Thus, we further characterized its properties towards in vivo applications.

Stability

The stability of **Pt1** was examined by ^{1}H and ^{195}Pt NMR. NMR of approximately 7 mM **Pt1** in DMSO-d_6 was recorded immediately after

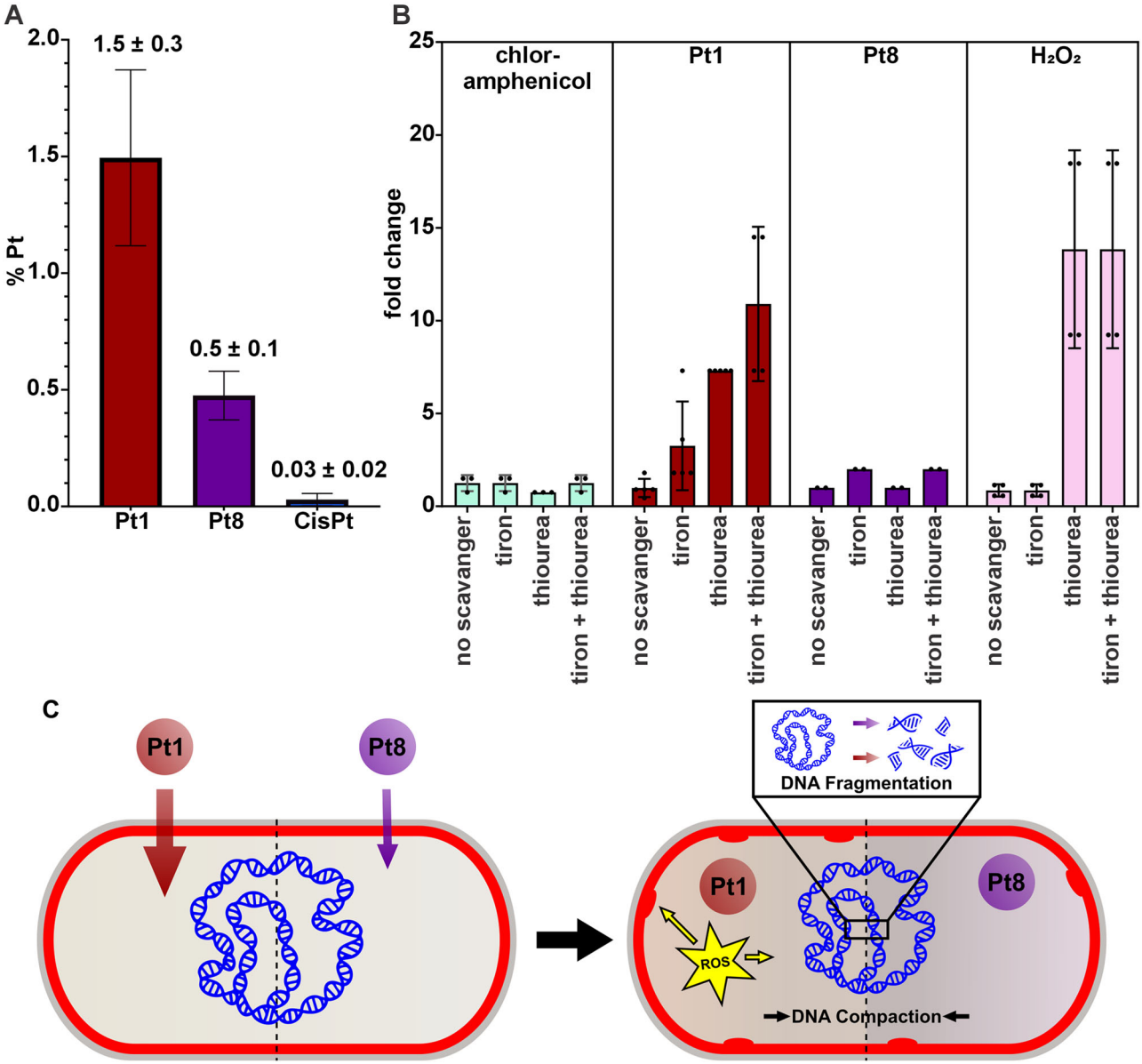

Fig. 6 | Compound uptake and ROS play a role in the increased potency of Pt1 compared to Pt8. A Percent Pt content of MRSA cell lysate after 60 min treatment with **Pt1, Pt8**, and **CisPt**. **B** MIC fold changes (increase) in the presence of ROS scavengers compared to regular medium without scavengers). Error bars represent standard deviation of at least three biological replicates. **C** Mode of action model based on phenotypic analysis of *B. subtilis*. Both Pt compounds damage DNA, causing DNA strand breaks and fragmentation, resulting in nucleoid compaction and reduced DAPI staining. **Pt1** additionally generates ROS, mainly hydroxyl radicals, further increasing its potency through multimodal cell damage, e.g., on the cell membrane.

preparation, and after 24 h and 48 h of incubation at 37 °C (Fig. S13–14). No differences in the NMR spectra could be identified, suggesting that **Pt1** remains intact for at least 48 h under the tested conditions.

The stability of **Pt1 and Pt8** in aqueous environment were examined by ^{1}H-NMR in the presence of 10% D_2O. No differences in the NMR spectra could be identified, suggesting that **Pt1** and **Pt8** remain intact for at least 24 h under the tested conditions (Figs. S15 and 16).

Combination with other antibiotics

Due to its unique DNA-targeting effect, we aimed to study whether **Pt1** could synergistically interact with approved antibiotics. We conducted a combination study with nine antibiotics commonly used against *S. aureus* (ATCC 29213). Neither synergistic nor antagonistic effects were observed with any of the tested antibiotics, indicating that the mode of growth inhibition of **Pt1** is unrelated to that of other antibiotics (Table S8).

Resistance development

We then explored the potential of **Pt1** to induce resistance in *S. aureus* (ATCC 29213), by growing the culture in the presence of compound at ½ MIC for 36 days. Only a minimal increase in the MIC (0.125 to 0.25 μg/mL) was observed over this time period, which is in stark contrast to a 256x fold MIC increase of the antibiotic levofloxacin under the same conditions (Fig. 7A).

We then used the strain resulting from 36 passages to interrogate whether cross-resistance to other antibiotics could be observed (Table S9). As expected, based on the preceding combination study and the very low resistance, no cross-resistance was observed, further emphasizing the unique nature of the mechanism of **Pt1**.

The efficacy of **Pt1** in suppressing bacterial growth after a brief exposure to the compound was assessed by studying its post-antibiotic effect (PAE). **Pt1** displayed a PAE of ~5.5 h compared to the control drugs levofloxacin and vancomycin, which displayed PAEs of 1.5 h and 2.5 h,

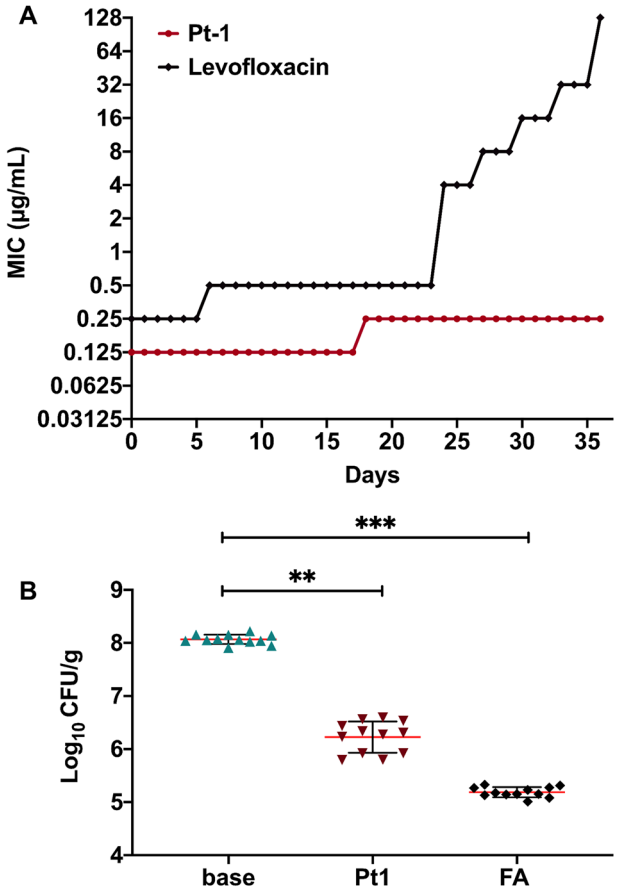

Fig. 7 | Resistance development and in vivo efficacy of Pt1. A Growth pattern of *S. aureus* ATCC 29213 grown in the presence of **Pt1** and levofloxacin at 0.5x MIC for 36 days. **B** Reduced bacterial load in an in vivo skin infection model in mice. Fusidic acid (**FA**) was used as positive control.

respectively, at 10x MIC (Table S10). Taken together, **Pt1** exhibits a long PAE while not inducing resistance, thus positively impacting its dosing regimen.

In vivo skin infection model

Following establishment of a favorable biological profile for **Pt1**, we proceeded to evaluate its efficacy in a topical *S. aureus* skin infection model (Fig. 7B). To this end, 5–7 weeks-old Swiss mice (22–25 g) were given a superficial wound on the dorsal surface, followed by infection with a bacterial load of ~10^7 CFU/mL. Mice treated with a 2% **Pt1** cream formulation displayed a ~ 1.9 $\log_{10}$ CFU/g reduction in bacterial load compared to the mice in the vehicle-treated group. Thus, **Pt1** reduced the bacterial load to an extent that is comparable to the established treatment (fusidic acid, ~2.9 $\log_{10}$ CFU/g). This experiment demonstrated the antibacterial in vivo efficacy of a platinum-containing compound in a mouse model.

Discussion

In the search for novel classes of antimicrobial agents we have identified platinum cyclooctadiene complexes with promising activity against Gram-positive bacteria and low toxicity against healthy human cells. Structure-activity relationship studies in this and previous work revealed several key insights. The halogen ligands on the platinum center seem to be crucial as alteration to methyl or hydroxy-containing ligands led to reduced activity and/or increased toxicity[32]. More scope remains to explore the effect of other, potentially bidentate, ligands (in conjunction with the COD) on the antibacterial activity and toxicity of these compounds. Switching the metal center to palladium was shown to result in complete loss of antibacterial properties and significant hemolysis[32], letting us conclude that the platinum is key. Finally, in this work, we explored the synthetically more challenging modifications of the COD ligand. Initially, we focused on modifications at the double bond to investigate how substitution at this position influences biological activity of this compound class. **Pt2**-**Pt5** were designed to investigate how variations in ligand electronics and steric properties influence the antibacterial activity of the resulting platinum complexes. The selected aromatic substituents were intended to provide a small but representative range of electronically and structurally distinct motifs, rather than to constitute a systematic substituent screening study. Accordingly, a phenyl group (**Pt2**), a meta-substituted aniline derivative (**Pt3**), and a para-benzaldehyde derivative (**Pt4**) were chosen as representative aryl systems bearing functional groups with different electronic characteristics and substitution patterns. This selection enabled us to assess whether both substituent identity and substitution position influence complex formation and/or biological activity. In addition, a furan derivative (**Pt5**) was included as a simple heteroaromatic motif to evaluate whether replacing a phenyl-type aromatic system with a heterocycle alters the behavior of the complex. We observed that any modification of the ligand at the double bond position resulted in loss of antibacterial activity in the final platinum compound. Therefore, further double-bond modifications were not pursued. Subsequently, a small series of allylic ether complexes (**Pt6**-**Pt10**) was prepared to explore how variation at the allylic position influences the properties and antibacterial activity of the complexes. Within this series, we examined the effect of aliphatic chain length ($n = 2$ for **Pt6** and $n = 3$ for **Pt7**), the introduction of a heteroatom-containing substituent (**Pt8**), and aromatic substitution at the allylic position (**Pt9** and **Pt10**). This approach allowed us to probe how steric bulk, lipophilicity, and electronic variation at the allylic position affect the behavior and biological activity of the resulting platinum complexes. Modification on the allylic COD position maintained some of the antibacterial properties. However, the best modified complex, **Pt8** was still significantly less active than the original hit-compound **Pt1**. Further expansion of these ligand series was not pursued at this time. This was motivated both by the significant synthetic challenges associated with the preparation and purification substituted Pt complexes, and because the biological results obtained for new derivatives of the present series were not sufficiently promising to justify a more extensive derivatization study at this stage. Both **Pt1** and **Pt8** showed broad activity against a range of clinical isolates of drug-resistant *S. aureus* and low cytotoxicity and hemolysis values. The structural similarity of **Pt1** with the anticancer drug **CisPt** prompted us to re-examine the antibacterial properties of the latter, which had been noted to induce bacterial elongation in the past[24]. In our hands, **CisPt** showed no antibacterial activity up to 100 µM against any of the evaluated bacterial strains. However, we did observe slight growth defects and a mild cell elongation phenotype in *B. subtilis* treated with 100 µM **CisPt** (Fig. S15). Uptake studies suggest that its poor activity is partially due to inefficient membrane translocation of the compound. Indeed the group of Nolan has shown that coupling platinum chemotherapeutics to siderophores leads to significant antibacterial activity [58,59].

We examined the antibacterial mechanisms of action of the lead compounds using BCP, which revealed clear effects on the bacterial DNA. **Pt1** additionally caused a noticeable, yet not significant formation, of Nile red foci in the cell membrane. Thorough investigation of the effects of **Pt1** and **Pt8** on membrane integrity and potential as well as on cell wall synthesis and cell division returned negative. Similarly, no distinct phenotype on fluorescent transcription and translation reporters could be observed, letting us conclude that these platinum compounds do not affect bacterial protein production. Taken together, these results indicate that the main target of both **Pt1** and **Pt8** is bacterial DNA.

Closer investigation of this target, through RecA as reporter for induction of the SOS response to DNA damage, revealed that both **Pt1** and **Pt8** induce a rapid response at 10 min after treatment that drops off over time. This is distinct from **CisPt**, which induces an increasing response over the 60 min measurement period. Importantly, we could demonstrate that all three platinum compounds are able to directly cause DNA fragmentation

using single-molecule imaging of fluorescently labeled λ-DNA. This effect was milder for **Pt1** compared to **Pt8**.

Studying the effect of different ROS quenchers on the antibacterial activity of the hit compounds revealed that the activity of **Pt1** is strongly suppressed in the presence of a hydroxyl radical scavenger. While a superoxide quencher alone did not affect activity, addition of both quenchers together achieved an even stronger reduction in **Pt1** activity, suggesting that hydroxyl radicals considerably contribute to its activity while superoxide may play a secondary role. In contrast, the activity of **Pt8** was not affected by any ROS quenchers.

Taken together, we propose a mode of action model for this new compound class (Fig. 6C). Both **P1** and **Pt8** directly bind to and damage bacterial DNA, leading to strand breaks and consequently DNA fragmentation. While **Pt8** is the more efficient DNA damaging agent, **Pt1** shows higher antibacterial activity. This seeming conundrum can be explained by (i) more efficient compound uptake, **Pt1** being taken up 50x more efficiently than **CisPt** and 3x more efficiently that than **Pt8**, and (ii) by an additional mechanism of **Pt1**, namely the generation of ROS. This multimodal effect of **Pt1** further explains its tendency to induce membrane stress (Nile red membrane foci), possibly through lipid peroxidation, as well as the absence of any high-level resistance emerging over 36 passages.

Finally, we evaluated the ability of **Pt1** to treat a topical *S. aureus* skin infection in a mouse model and observed a ~ 1.9 $\log_{10}$ CFU/g reduction in bacterial load. Altogether, these observations make **Pt1** a highly interesting lead compound with potent activity against critical antibiotic-resistant pathogens, low cytotoxicity, a unique and multimodal mechanism of action that does not permit effective resistance development, and potent efficacy in an in vivo mouse infection model. In terms of their antibacterial properties, **Pt1** compares favorably with other recently reported metalloantibiotics which generally show MICs in the same range[60,61]. However, observation that these compounds are only applicable in topical infections limits their clinical translatability. Further developments could lead to a compound with more favorable properties that make it amenable to systemic infections. This and our previous studies[32] have explored modification of the halide ligands, substitution for the platinum metal with palladium and now chemical modification of the COD ligand. In general, any deviation from the original **Pt1** has led to a reduction in antibacterial activity and no significant improvement in other important physicochemical properties such as solubility. There is still scope for modifications, for example bidentate ligands could be used to replace the two halides, as has been done in oxaliplatin[62] and carboplatin[63]. Changing the COD ligand to other chemically more versatile dienes could also be explored. Potentially the pivot to Pt(IV) complexes in a pro-drug approach could also be explored as has been done by Guo et al. recently [58].

In general, DNA is an underexplored antibacterial target and only few antibiotics that specifically target DNA in bacteria are on the market[64]. Metal compounds such as ruthenium polypyridyl complexes have long been known to intercalate DNA through non-covalent interactions[65,66]. The herein-reported class of platinum compounds represents the first non-cisplatin-based compounds with a demonstrated direct DNA effect, high selectivity for bacteria and in vivo efficacy, validating further explorations into the development of platinum compounds as new antibiotic class with a highly attractive biological profile.

Methods

Syntheses of COD ligands and Pt(II) complexes

The detailed synthetic procedures and characterization of compounds can be found in the supplementary information (S1**. General Material** and S2**. Synthetic Procedures**).

Antibiotic susceptibility testing of lead compounds

Determination of antibacterial activity: Minimum inhibitory concentration assay. The MIC protocol was adapted from Cai et al[67]. A single colony of bacteria was grown in Luria-Bertani (LB) medium overnight at 37 °C. Stock solutions of 5 mM of the samples were prepared in DMSO and diluted to a starting concentration of 100 μM in Mueller Hinton (MH) medium. The overnight culture was diluted and incubated until the OD_{600} reached 0.6–1.0. The bacteria concentration was measured by measuring the optical density at 600 nm and diluted to an OD_{600} of 0.022 in MH medium. 5 μL of the diluted bacterial solution was used to inoculate 150 μL of the sample solutions, resulting in a final inoculation of about 5×10^5 cells/mL. The plates were then incubated at 37 °C for 18 h. For each assay, a control of broth only and a growth control of broth with bacterial inoculum without antibiotics were included in two columns of the plate. Polymyxin B and vancomycin were used as control antibiotic for *E. coli*, MRSA, *B. subtilis*, and MSSA, respectively. The growth was measured by analysing the absorbance of the bacterial suspension at 600 nm. Each experiment was performed in triplicate.

Determination of antibacterial activity: Minimum inhibitory concentration assay against selection of Gram-positive and Gram-negative strains[68]. The data is given in supporting information (Table S5). Before starting the experiment, a single colony was picked from MHA plate, inoculated in MHBII and incubated overnight at 37 °C with shaking for 18–24 h to get the starter culture. Antibiotic susceptibility testing was conducted according to the CLSI (Clinical & Laboratory Standards Institute) guidelines using the broth microdilution assay. 10 mg/mL stock solutions of test compounds were prepared in DMSO. Bacterial cultures were inoculated in MHBII and optical density (OD) was measured at 600 nm, followed by dilution to achieve ~10^6 CFU/mL. The compounds were tested from 64 to 0.5 mg/L in two-fold serial diluted fashion with 2.5 μL of each concentration added to well of a 96-well round bottom microtiter plate. Later, 97.5 μL of bacterial suspension was added to each well containing either test compound or appropriate controls. The plates were incubated at 37 °C for 18–24 h following which the MIC was determined. The MIC is defined as the lowest concentration of the compound at which there is absence of visible growth. For each test compound, MIC determinations were carried out independently three times using duplicate samples.

Determination of hemolytic activity in hRBCs: hemolysis assay. The compounds were tested on human red blood cells (hRBCs) using a hemolysis assay, adapted from previously published procedure[69]. 1.5 mL of whole blood was centrifuged at 3000 rpm for 15 min at 4 °C, and the plasma was discarded. The hRBC pellet was washed three times with PBS (pH 7.4) and then resuspended to a final volume of 10 mL in PBS. For the determination of HC_{50} of the lead compounds, the samples serially diluted starting from 200 μM. Samples stock solution was 5 mM in DMSO. Each plate included a blank medium control (PBS) and a hemolytic activity control (0.1% Triton TM X-100). The hRBC suspension was incubated with the samples in PBS in a V-shaped 96-well plate for 4 hours at 20 °C. After the incubation, 100 μL of supernatant was carefully pipetted to a flat bottom, clear 96-wells plate. Hemolysis was measured by analysing the absorbance at 540 nm using a plate reader. The percentage of hemolysis at each concentration was determined and the HC_{50} was calculated by inhibitor vs. normalized response fit. The hemolytic activity was measured by analysing the absorbance of free hemoglobin in the supernatants at 540 nm. Minimum inhibitory concentration (MHC) was determined by eye. Each experiment was repeated in triplicate.

Determination of cytotoxicity of lead compounds against HEK293T cells[67]. Stock solutions of 5 mM of the compounds were prepared in DMSO and the stock solution of cisplatin and oxaliplatin were prepared in 1% NaCl as 4.3 mM and 2.5 mM respectively. The control for the experiments was DMSO. HEK293T cells were cultivated in DMEM high glucose supplemented with 10% heat-inactivated fetal bovine serum, 100 U/mL of penicillin and streptomycin and maintained at a temperature of 37 °C with 5% CO_2. Initially, 4000/well of cells were seeded into 96-well plates and incubated for 24 h before being exposed to compounds at concentrations ranging from 0.78, 50, and 100 μM. After

24 h of incubation, the compounds were added and serially diluted and incubated for 24 and 48 h at 37 °C 5% CO_2, the cells were stained with alamar Blue, and the fluorescence excitation/ emission 540 nm/590 nm was measured using 96 well-plate reader. CC_{50} is defined as the lowest concentration of compound which leads to a 50% reduction in cell viability compared to untreated and DMSO control. Each experiment was repeated in triplicate.

Determination of cytotoxicity of lead compounds against vero cells. Cell toxicity was performed against Vero cells using the MTT assay[70]. ~10^3 cells/well were seeded in 96 well plate and incubated at 37 °C with 5% CO_2 atmosphere. After 24 h, compound was added ranging from 100 to 12.5 μg/mL concentration and incubated for 72 h. After the incubation was over, MTT was added in each well, incubated at 37 °C for further 4 h, residual medium was discarded, 0.1 mL of DMSO was added to solubilize the formazan crystals and OD_{540} was taken for the calculation of IC_{50}. Doxorubicin was used as positive control and each experiment was repeated in triplicate.

Bacterial strains and growth conditions for mode of action analysis: Determination of optimal stressor concentrations (OSC)

To establish a starting concentration for the OSC assay, MICs against parent strain 168CA were determined under conditions equivalent to those used for mode of action assays. MICs were determined according to the Clinical Laboratory Standardization Institute (CLSI) in a serial microdilution assay[52]. The compounds were serially 2-fold diluted in a 96-well plate and *B. subtilis* (168CA) was added to a final cell count of 5×10^5 CFU/mL. Cultures were incubated for 16 h at 37 °C under constant agitation. MICs were used as basis for OSC determination. To this end, growth curves were recorded using optical density (OD) measurements. Culture volumes of 20 mL were grown until reaching an OD_{600} of 0.3. Subsequently, the parent culture was split into 2 ml aliquots, followed by addition of different MIC multiples of Pt compounds[71]. An untreated culture served as control. Growth was followed until cultures reached the stationary phase. A concentration achieving 50–70% growth inhibition in exponential phase was selected as optimal stressor concentration. The following concentrations were selected: 3.125 μg/mL **Pt1**, 25 μg/mL **Pt8**, 100 μM **CisPt**. As controls, 0.23 μM nisin, 0.53 μM μM gramicidin, 100 μM CCCP, 0.67 μM vancomycin, 1.2 μM rifampicin, and 323.12 μM chloramphenicol were included as controls for specific assays as appropriate.

Fluorescence light microscopy

Microscopy images of bacteria were acquired on a Nikon Eclipse Ti2 equipped with a CFI Plan Apochromat DM Lambda 100X Oil objective (N.A. 1.45, W.D. 0.13 mm), a Photometrics PRIME BSI camera, a Lumencor Sola SE II FISH 365 light source, and an Okolab temperature incubation chamber. Images were obtained using the NIS elements AR software version 5.21.03/5.42.02. DNA stretching images were obtained on a Zeiss Observer.Z1 fluorescence microscope equipped with a Colibri 7 LED illumination system and an Andor iXON Ultra EMCCD camera. Image analysis was perfomred using ImageJ[72], MicrobeJ[73], and ObjectJ[74,75].

Bacterial cytological profiling (BCP)[71]

BCP was performed according to Wenzel et al.[71]. In short, *B. subtilis* strain MW54 (*PrpsD-gfp*) was grown to an OD_{600} of 0.3 prior to splitting of parent cultures and addition of antibiotics. Samples were taken for microscopy after 30, 60, and 120 min of antibiotic treatment. Five minutes prior to sampling, cultures were stained with 0.5 μg/mL Nile red and 1 μg/mL DAPI for 5 min. Samples of 0.5 μL were then spotted onto 1% agarose slides[45] and images were taken immediately.

BCP image analysis

Cell length and DAPI intensity were analyzed using MicrobeJ[73]. To this end, the fit shape, rod-shaped setting was used with a minimum area of 0.5 μm, while all other settings remained at default. *B. subtilis* chains were seperated based on the membrane stain. Membrane stress was counted using the ObjectJ plugin[74], using the membrane setting to seperate individual cells in chains. Membrane damage was expressed as ratio of cells with visible Nile red foci and total detected cells. DNA compaction was analyzed by determining the area of the DNA and the whole cell are using advanced weka segmentation. Cells were segmented according to the GFP signal. Automatic segmentation that did not fit the DNA or cell shape was corrected by manual tracing. Cells that were out of focus or lysed were excluded from the analysis. Statistical analysis was peformed using GraphPad Prism 10 as specified in the individual figure legends.

Propidium iodide pore assay[71]

Propidium iodide staining was performed as described previously. *B. subtilis* 168CA was grown to an OD_{600} of 0.3 prior to splitting of the parent culture and treatment with the different antibiotics. After 15 and 45 min, samples were stained with 13.3 μg/mL propidium iodide for 15 min (total treatment times 30 and 60 min), and washed 3 times with phosphate-buffered saline (PBS). Fluorescence signals were recorded at an excitation wavelength of 535–15 nm and an emission wavelength of 617–20 nm in a BMG Clariostar Plus plate reader.

$DiSC_3(5)$-based membrane potential measurements[71]

The membrane potential was measured according to Winkel et al. with minor modifications[45]. *B. subtilis* 168CA was grown in LB containing 50 μg/mL bovine serum albumin (BSA). Cells were transferred to black 96-well polystyrene microtiter plates after reaching an OD_{600} of 0.3. $DiSC_3(5)$ was added to a final concentration of 1 μM, maintaining a constant concentration of 1% DMSO to avoid precipitation of the dye. After the fluorescence baseline had stabilized, antibiotic compounds were added, and measurements were continued for 30 min. Fluorescence was recorded at an excitation wavelength of 610–30 nm and an emission wavelength of 675–50 nm in a BMG Clariostar Plus plate reader.

GFP localization studies[41]

B. subtilis strains were grown in LB containing appropriate inducer concentrations as specified in Table S10. After reaching an OD_{600} of 0.3, cultures were split and treated with antibiotics. Samples were withdrawn after 30 and 60 min of treatment, spotted on glass slides covered with 1% agarose films[45], and immediately imaged.

Translation inhibition assay

B. subtilis strain TB35 (*Pxyl-minD-gfp*) was grown in LB without inducer. After reaching an OD_{600} of 0.3, antibiotics and inducer (0.1% xylose) were added consecutively. Samples were withdrawn for microscopy after 60 min of treatment, spotted on glass slides covered with 1% agarose films, and imaged without delay.

Single-molecule imaging of DNA

DNA stretching was performed on silanized glass coverslips (18×18 mm^2) using a silanization protocol adapted from Wei et al.[76]. Briefly, glass coverslips were arranged in a coverslip rack and submerged overnight in acetone solution containing 1% APTES and 1% ATMS (v/v). The activated coverslips were then rinsed with a (2:1 v/v) acetone:water solution and dried with air purging. Prior to imaging, 138.6 ng of λ-DNA were treated with the respective compounds for 10 min, followed by staining with 320 nM YOYO-1 in 0.5× Tris-borate-EDTA (TBE) buffer. To minimize photobleaching, 2% β-mercaptoethanol (BME) was added. 3.2 μL of the stained DNA sample were placed at the interface between a silanized coverslip and a clean microscope slide to stretch the DNA molecules. A band-pass excitation filter (475/40 nm) and a band-pass emission filter (530/50 nm) were used for detecting YOYO-1 fluorescence.

DNA length analysis

To analyse the length of individual DNA molecules, the ImageJ[72] plugin MicrobeJ[73] was used. DNA molecules were detceted using medial axis

detection with 1 μm minimum length, 0.3 to 1.5 μm width range with 0–0.04 variation, and a maximum circularity value of 0.7. DNA molecules that were not correctly detected were selected manually. DNA length measurements were analyzed and visualized with Origin 2023.

ROS scavenger assay

LB media were prepared to contain either 10 mM tiron, 150 mM thiourea, 10 mM tiron and 150 mM thiourea, or no scavanger. Serial two-fold dilutions of the different antibiotics were prepared in the respective media and transferred to 96-well plates. *B. subtilis* 168CA was added to a final cell count of 5×10^5 CFU/mL and cultures were incubated at 37 °C for 16 h under constant agitation. The OD_{600} was meassured in a BMG Clariostar Plus plate reader.

Antibiotic uptake assay[53]

A single colony of bacteria was grown in Luria-Bertani (LB) medium overnight at 37 °C. Stock solutions of 5 mM of the samples were prepared in DMSO for **Pt1** and **Pt8**, and 5.3 mM in 0.9% $NaCl_{(aq)}$ for **CisPt**. The overnight culture was diluted in 80 mL LB medium and grown until it reached an OD_{600} of 0.3–04. 10 mL of the culture were distributed to falcon tubes and cells were stressed with 1.56 μM **Pt1**, 6.25 μM **Pt8** and 100 μM **CisPt** for 30 and 60 min. Then, the cells were harvested at 4500 rpm for 10 min and the supernatant was collected. The cell pellets were washed with 1 mL washing buffer (100 mM Tris, 1 mM EDTA, pH 7.3) and centrifuged at 4500 rpm for 10 min each. Subsequently, cell pellets were resuspended in 1 mL PBS (pH 7.5), treated with 500 μL lysing buffer (0.1 M glycine-HCl, pH 2.5), and incubated overnight at room temperature. Following incubation, samples were centrifuged at 14,000 rpm for 5 min and supernatant (cell lysis) and pellet (cell debris) were collected. After pellets were resuspended in 750 μL PBS (pH 7.5), all samples were frozen in liquid N_2 and lyophilized overnight. Then, samples were treated with 300 μL nitric acid (69.7% (w/mL) in double-distilled water) and incubated for a week at room temperature, followed by incubation at 65 °C for 4 h. Then, the samples were diluted to 2% nitric acid content with double-distilled water and filtered through 0.22 μm syringe filters.

The ICP-MS system was operated in kinetic energy discrimination (KED) mode and the collision gas was He50 (AlphaGaz), pre-treated with a helium cell gas filtration system (Perkin Elmer, N8146004). The gas flow for KED was 5.3 mL/min. 2% HNO_3 (*w/w*) was used as matrix for all sample, calibration, and internal standard (IS) solutions. 2% HNO_3 (*w/w*) itself was prepared from 69.3% (*w/w*) HNO3 (BASF, <1 ppb ECME), diluted with ultrapure water ($\rho = 18.2$ MΩ+cm). Calibration solutions of 0.1, 1, 10 and 50 μg/L Mg, Mn, and Pt were prepared. For Mg and Mn, the 'ICP multi-element standard solution VIII' (Merck, 1.09492) was used as a stock solution. 'Platinum Standard for ICP' (Sigma-Aldrich, 19078) was used as a stock solution for Pt. All elements were combined in the same calibration solutions. 20 μg/L Ir and 20 μg/L Y in 2% HNO_3 were used as internal standards (IS) during the ICP-MS analysis. Y was used as IS for Mg and Mn. Ir was used as IS for Pt. Stock solutions were 'Iridium ICP standard' (Supelco, 1.70325) and 'Yttrium ICP standard' (Merck, 1.70368). Both elements were combined in the same IS solutions. The respective isotopes measured were: ^{24}Mg, ^{26}Mg, ^{55}Mn, ^{89}Y, ^{195}Pt, and ^{193}Ir. Each sample measurement consisted of 7 replicates and no automatic corrections for potential interferences were applied.

Determination of Pt1 and Pt8 stability

The stability of **Pt1** complex was measured by ^1H and ^{195}Pt NMRs. Approximately 7 mM of **Pt1** in DMSO-d_6 was prepared and NMR spectra were immediately measured. Measurements were repeated after the 24 h and 48 h of incubations at 37 °C.

The stability of **Pt1** in aqueous environment was examined by ^1H NMR. NMR of approximately 15 mM **Pt1 and** 6 mM **Pt8** in DMSO-d_6 was recorded immediately after preparation. Then, 10% D_2O was added and 1H NMR was recorded immediately and after 24 h of incubation at 37 °C.

Drug interaction study

Interaction of **Pt1** with FDA-approved antibiotics was determined using chequerboard assays following CLSI guidelines. All compounds were freshly prepared for the experiment. Eight serial two-fold dilutions of **Pt1** were prepared from 1 to 0.0078 μg/mL. Test antibiotics were prepared in 12 serial two-fold dilutions as follows: ceftazidime 64–0.03125 μg/mL, daptomycin and vancomycin 8–0.0039 μg/mL, gentamicin, levofloxacin, meropenem, and minocycline 2–0.00095 μg/mL, linezolid 16–0.0078 μg/mL, rifampicin 0.06–0.000014 μg/mL. Dilution series were inoculated with 5×10^5 *S. aureus* ATCC 29213 CFU/mL and incubated for 16–20 h at 37 °C. Following incubation, the fractional inhibitory concentration index (FICI) was calculated with the formula FICI = FICA + FICB, whereby FICA = MIC of drug A in combination/MIC of drug A alone and FICB = MIC of drug B in combination/MIC of drug B alone. A drug combination is considered synergistic when ∑FICI is ≤0.5, indifferent when ∑FICI is >0.5 to 4, and antagonistic when ∑FICI is >4.

Postantibiotic effect

Post antibiotic effect (PAE) was determined as follows. Overnight culture of *S. aureus* ATCC 29213 were diluted in MHBII to ~10^5 CFU/mL, exposed to 1x and 10x MIC of **Pt1**, levofloxacin, and vancomycin, and incubated at 37 °C for 1 h. Following incubation, cultures were centrifuged and washed twice with pre-warmed MHBII to remove any traces of antibiotics. Finally, cells were resuspended in drug-free MHBII and incubated further at 37 °C. Samples were taken every 1 h, serially diluted, and plated on tryptic soy agar (TSA) for enumeration of CFU. PAE was calculated as PAE = T – C; where T is the difference in time required for 1 log10 increase in CFU vs. CFU observed immediately after the removal of the drug, and C in a similarly treated drug-free control.

Resistance induction[76]

S. aureus ATCC 29213 was serially passaged in the presence of 0.5×MIC of either **Pt1** or levofloxacin (positive control). The MICs of the passaged cultures were determined every 3 days and compared to that of wild type *S. aureus* ATCC 29213. MIC changes were recorded for 36 passages.

Murine skin infection model[77]

The in vivo efficacy of **Pt1** was determined in a superficial skin infection model. Briefly, male Swiss mice, 4–6 weeks old, weighing ~22–25 g, were used throughout the study. Mice were caged alone in an individually vented cage (IVC) to check cross-contamination and to maintain aseptic conditions throughout the experiment. Ketamine and xylazine were prepared in distilled water, 40 mg/kg and 8 mg/kg of body weight, respectively, and injected intraperitoneally (IP) as a mixture of 100 μL in each mouse for anaesthesia. Then, we proceeded with the removal of fur by applying depilatory cream. The area was cleaned with sterile distilled water. Approximately 2 cm^2 of skin area was scratched until it became visibly reddened and glistening without any bleeding. For bacterial infection, a 10 μL droplet containing 10^7 CFU/mL of *S. aureus* ATCC 29213 was applied to the reddened area of skin. To confirm the infection, post 4 h, untreated mice were sacrificed, skin homogenized, and various dilutions of the treatment groups (6 mice per group) were plated on TSA plates. Following this, treatment with 2% fusidic acid (positive control), 2% **Pt1**, and base (vehicle) was started, followed by a second dose post 16 h from the first dose. Henceforth, the drug regimen was comprised of twice daily application (in the morning and the evening, with an 8 h interval) for 4 days. Control mice were regularly treated with 25–30 mg each of 2% fusidic acid (LEO Pharma, Ballerup, Denmark), 2% infuzide, and base (vehicle). All groups were sacrificed post-18 h of the last dose to avoid carryover effects of the treatment group. Around ~2 cm^2 of wounded skin were excised post sacrifice and homogenized in 500 μL PBS in 2 mL MP tissue grinding Lysing Matrix F tubes using MP FastPrep-24 set at 4.0 M/S for 30 s (3 cycles). Dilutions were plated post homogenization on TSA plates, followed by overnight incubation at 37 °C, to determine the bacterial CFU count in each treatment group. Each experiment was repeated three times in duplicate and the mean and SEM of Log_{10} CFU/g were plotted.

Data availability

All data supporting the findings of this study are available within the paper and its Supplementary Information.

Received: 13 December 2025; Accepted: 20 April 2026;
Published online: 08 May 2026

References

1. Tang, K. W. K., Millar, B. C. & Moore, J. E. Antimicrobial Resistance (AMR). *Br. J. Biomed. Sci.* **80**, 11387 (2023).
2. Murray, C. J. L. et al. Global burden of bacterial antimicrobial resistance in 2019: a systematic analysis. *Lancet* **399**, 629–655 (2022).
3. Butler, M. S., Henderson, I. R., Capon, R. J. & Blaskovich, M. A. T. Antibiotics in the clinical pipeline as of December 2022. *J. Antibiot.* **76**, 431–473 (2023).
4. Inc, N. T. U. Nabriva Therapeutics Announces European Medicines Agency (EMA) validation of marketing authorization application for Lefamulin. *GlobeNewswire News Room*. Accessed 25 March 2026 https://www.globenewswire.com/news-release/2019/06/24/1873292/37424/en/Nabriva-Therapeutics-Announces-European-Medicines-Agency-EMA-Validation-of-Marketing-Authorization-Application-for-Lefamulin.html.
5. Hu, S., Yu, H. & Gao, J. Gepotidacin: The first-in-class triazaacenaphthylene antibiotic approved for the treatment of uncomplicated urinary tract infections. *Drug Discov. Ther.* **19**, 129–130 (2025).
6. Lang, K. Why the approval of two new gonorrhoea treatments is a game changer. *BMJ* **392**, r2684 (2026).
7. Lipinski, C. A., Lombardo, F., Dominy, B. W. & Feeney, P. J. Experimental and computational approaches to estimate solubility and permeability in drug discovery and development settings. *Adv. Drug Deliv. Rev.* **23**, 3–25 (1997).
8. Cooper, M. A. A community-based approach to new antibiotic discovery. *Nat. Rev. Drug Discov.* **14**, 587–588 (2015).
9. Frei, A. et al. Metal complexes as a promising source for new antibiotics. *Chem. Sci.* **11**, 2627–2639 (2020).
10. Lovering, F., Bikker, J. & Humblet, C. Escape from Flatland: increasing saturation as an approach to improving clinical success. *J. Med. Chem.* **52**, 6752–6756 (2009).
11. Gasser, G. & Metzler-Nolte, N. The potential of organometallic complexes in medicinal chemistry. *Curr. Opin. Chem. Biol.* **16**, 84–91 (2012).
12. Morrison, C. N. et al. Expanding medicinal chemistry into 3D space: metallofragments as 3D scaffolds for fragment-based drug discovery. *Chem. Sci.* **11**, 1216–1225 (2020).
13. Hung, A. W. et al. Route to three-dimensional fragments using diversity-oriented synthesis. *Proc. Natl. Acad. Sci. USA* **108**, 6799–6804 (2011).
14. Ratia, C., Soengas, R. G. & Soto, S. M. Gold-derived molecules as new antimicrobial agents. *Front. Microbiol*. **13**, 846959 (2022).
15. Kabir, E., Noyon, M. R. O. K. & Hossain, M.dA. Synthesis, biological and medicinal impacts of metallodrugs: a study. *Results Chem.* **5**, 100935 (2023).
16. Pandey, A. & Boros, E. Coordination complexes to combat bacterial infections: recent developments, current directions and future opportunities. *Chem. - Eur. J.* **27**, 7340–7350 (2021).
17. Waters, J. E., Stevens-Cullinane, L., Siebenmann, L. & Hess, J. Recent advances in the development of metal complexes as antibacterial agents with metal-specific modes of action. *Curr. Opin. Microbiol.* **75**, 102347 (2023).
18. Llamedo, A., Cano, M., Soengas, R. G. & García-Alonso, F. J. Enhancing the therapeutical potential of metalloantibiotics using nano-based delivery systems. *Beilstein J. Nanotechnol.* **16**, 1350–1366 (2025).
19. Anthony, E. J. et al. Metallodrugs are unique: opportunities and challenges of discovery and development. *Chem. Sci.* **11**, 12888–12917 (2020).
20. Chattaraj, A., Syed, M. P., Low, C. A. & Owonikoko, T. K. Cisplatin-induced ototoxicity: a concise review of the burden, prevention, and interception strategies. *JCO Oncol. Pract.* **19**, 278–283 (2023).
21. Yamamoto, S. et al. A retrospective study on optimal number of cycles of the first-line platinum-based chemotherapy for metastatic urothelial carcinoma. *Urol. Oncol. Semin. Orig. Investig.* **40**, 194.e7–194.e14 (2022).
22. Rosenberg, B. et al. The inhibition of growth or cell division in *Escherichia coli* by different ionic species of platinum (IV) complexes. *J. Biol. Chem.* **242**, 1347–1352 (1966).
23. Ghosh, S. Cisplatin: the first metal based anticancer drug. *Bioorg. Chem.* **88**, 102925 (2019).
24. Johnstone, T. C., Alexander, S. M., Lin, W. & Lippard, S. J. Effects of monofunctional platinum agents on bacterial growth: a retrospective study. *J. Am. Chem. Soc.* **136**, 116–118 (2014).
25. Ortega, E. et al. A 2-(benzothiazol-2-yl)-phenolato platinum(II) complex as potential photosensitizer for combating bacterial infections in lung cancer chemotherapy. *Eur. J. Med. Chem.* **222**, 113600 (2021).
26. Kaur, M. et al. Antimicrobial efficacy of a hemilabile Pt (II)–NHC compound against drug-resistant *S. aureus* and *Enterococcus*. *Dalton Trans.* **52**, 1876–1884 (2023).
27. Lunagariya, M. V., Thakor, K. P., Kanthecha, D. N. & Patel, M. N. Synthesis, characterization and biological applications of substituted pyrazolone core based platinum(II) organometallic compounds. *J. Organomet. Chem.* **854**, 49–63 (2018).
28. Rivera, C. et al. *Cis* and *trans* platinum(II) N-heterocyclic carbene isomers: synthesis, characterization and biological activity. *N. J. Chem.* **46**, 14221–14226 (2022).
29. Yu, W. et al. Synthesis and characterization of neutral cyclometalated platinum(II) complexes and their antibacterial and cytotoxic evaluations. *Eur. J. Inorg. Chem.* **26**, e202200529 (2023).
30. Rubino, S. et al. Synthesis, properties, antitumor and antibacterial activity of new Pt(II) and Pd(II) complexes with 2,2′-dithiobis(benzothiazole) ligand. *Bioorg. Med. Chem.* **25**, 2378–2386 (2017).
31. Frei, A. et al. Metal complexes as antifungals? From a crowd-sourced compound library to the first in vivo experiments. *JACS Au* **2**, 2277–2294 (2022).
32. Frei, A. et al. Platinum cyclooctadiene complexes with activity against gram-positive bacteria. *ChemMedChem* **16**, 3165–3171 (2021).
33. Joyce, K. et al. Antimicrobial spectrum of the antitumor agent, cisplatin. *J. Antibiot.* **63**, 530–532 (2010).
34. Chowdhury, N., Wood, T. L., Martínez-Vázquez, M., García-Contreras, R. & Wood, T. K. DNA-crosslinker cisplatin eradicates bacterial persister cells. *Biotechnol. Bioeng.* **113**, 1984–1992 (2016).
35. Vaara, M. Agents that increase the permeability of the outer membrane. *Microbiol. Rev.* **56**, 395–411 (1992).
36. Faria, J., Ahmed, S., Gerritsen, K. G. F., Mihaila, S. M. & Masereeuw, R. Kidney-based in vitro models for drug-induced toxicity testing. *Arch. Toxicol.* **93**, 3397–3418 (2019).
37. Jahn, N., Brantl, S. & Strahl, H. Against the mainstream: the membrane-associated type I toxin BsrG from Bacillus subtilis interferes with cell envelope biosynthesis without increasing membrane permeability. *Mol. Microbiol.* **98**, 651–666 (2015).
38. Schäfer, A.-B. et al. Dissecting antibiotic effects on the cell envelope using bacterial cytological profiling: a phenotypic analysis starter kit. *Microbiol. Spectr.* **12**, e0327523 (2024).
39. Tanious, F. A., Veal, J. M., Buczak, H., Ratmeyer, L. S. & Wilson, W. D. DAPI (4',6-diamidino-2-phenylindole) binds differently to DNA and RNA: minor-groove binding at AT sites and intercalation at AU sites. *Biochemistry* **31**, 3103–3112 (1992).

40. Lenhart, J. S. et al. RecO and RecR are necessary for RecA loading in response to DNA damage and replication fork stress. *J. Bacteriol.* **196**, 2851–2860 (2014).
41. Schäfer, A.-B. et al. Dual Action of Eeyarestatin 24 on Sec-dependent protein secretion and bacterial DNA. *ACS Infect. Dis.* **9**, 253–269 (2023).
42. Aning, O. A. et al. Stained DNA Dot Detection (SD3): an automated tool for quantifying fluorescent features along single stretched DNA molecules. *DNA Repair* **149**, 103836 (2025).
43. Tchounwou, P. B., Dasari, S., Noubissi, F. K., Ray, P. & Kumar, S. Advances in our understanding of the molecular mechanisms of action of cisplatin in cancer therapy. *JEP* **13**, 303–328 (2021).
44. Bierbaum, G. & Sahl, H.-G. Lantibiotics: mode of action, biosynthesis and bioengineering. *Curr. Pharm. Biotechnol.* **10**, 2–18 (2009).
45. te Winkel, J. D., Gray, D. A., Seistrup, K. H., Hamoen, L. W. & Strahl, H. Analysis of antimicrobial-triggered membrane depolarization using voltage sensitive dyes. *Front. Cell Dev. Biol.* **4**, 29 (2016).
46. Kelkar, D. A. & Chattopadhyay, A. The gramicidin ion channel: a model membrane protein. *Biochim. Biophys. Acta* **1768**, 2011–2025 (2007).
47. Strahl, H. & Hamoen, L. W. Membrane potential is important for bacterial cell division. *Proc. Natl. Acad. Sci.USA* **107**, 12281–12286 (2010).
48. Wenzel, M. et al. Control of septum thickness by the curvature of SepF polymers. *Proc. Natl. Acad. Sci.USA* **118**, e2002635118 (2021).
49. Schirner, K. et al. Lipid-linked cell wall precursors regulate membrane association of bacterial actin MreB. *Nat. Chem. Biol.* **11**, 38–45 (2015).
50. Kamal El-Sagheir, A. M. et al. N4-substituted Piperazinyl Norfloxacin derivatives with broad-spectrum activity and multiple mechanisms on gyrase, topoisomerase IV, and bacterial cell wall synthesis. *ACS Bio. Med. Chem. Au* **3**, 494–506 (2023).
51. Errington, J., Daniel, R. A. & Scheffers, D.-J. Cytokinesis in bacteria. *Microbiol. Mol. Biol. Rev.* **67**, 52–65 (2003).
52. Saeloh, D. et al. The novel antibiotic rhodomyrtone traps membrane proteins in vesicles with increased fluidity. *PLoS Pathog.* **14**, e1006876 (2018).
53. Frei, A., Amado, M., Cooper, M. A. & Blaskovich, M. A. T. Light-activated rhenium complexes with dual mode of action against bacteria. *Chem. Eur. J.* **26**, 2852–2858 (2020).
54. Liu, T. Z., Lin, T. F., Chiu, D. T., Tsai, K. J. & Stern, A. Palladium or platinum exacerbates hydroxyl radical mediated DNA damage. *Free Radic. Biol. Med.* **23**, 155–161 (1997).
55. Cornelis, P., Wei, Q., Andrews, S. C. & Vinckx, T. Iron homeostasis and management of oxidative stress response in bacteria. *Metallomics* **3**, 540–549 (2011).
56. Gray, D. A. et al. Membrane depolarization kills dormant Bacillus subtilis cells by generating a lethal dose of ROS. *Nat. Commun.* **15**, 6877 (2024).
57. Checa, J. & Aran, J. M. Reactive oxygen species: drivers of physiological and pathological processes. *J. Inflamm. Res.* **13**, 1057–1073 (2020).
58. Guo, C., Wang, K.-K. A. & Nolan, E. M. Investigation of Siderophore–Platinum(IV) conjugates reveals differing antibacterial activity and DNA damage depending on the platinum cargo. *ACS Infect. Dis.* **10**, 1250–1266 (2024).
59. Guo, C. & Nolan, E. M. Heavy-metal trojan horse: enterobactin-directed delivery of platinum(IV) prodrugs to *Escherichia coli*. *J. Am. Chem. Soc.* **144**, 12756–12768 (2022).
60. Smitten, K. L. et al. Using nanoscopy to probe the biological activity of antimicrobial leads that display potent activity against pathogenic, multidrug resistant, gram-negative bacteria. *ACS Nano* **13**, 5133–5146 (2019).
61. Sovari, S. N. et al. Combatting AMR: a molecular approach to the discovery of potent and non-toxic rhenium complexes active against *C. albicans*-MRSA co-infection. *Eur. J. Med. Chem.* **226**, 113858 (2021).
62. O'Dowd, P. D., Sutcliffe, D. F. & Griffith, D. M. Oxaliplatin and its derivatives – An overview. *Coord. Chem. Rev.* **497**, 215439 (2023).
63. Kelland, L. The resurgence of platinum-based cancer chemotherapy. *Nat. Rev. Cancer* **7**, 573–584 (2007).
64. Bolhuis, A. & Aldrich-Wright, J. R. DNA as a target for antimicrobials. *Bioorg. Chem.* **55**, 51–59 (2014).
65. Frei, A., Verderosa, A. D., Elliott, A. G., Zuegg, J. & Blaskovich, M. A. T. Metals to combat antimicrobial resistance. *Nat. Rev. Chem.* **7**, 202–224 (2023).
66. Smitten, K. L. et al. Mononuclear ruthenium(II) theranostic complexes that function as broad-spectrum antimicrobials in therapeutically resistant pathogens through interaction with DNA. *Chem. Sci.* **11**, 8828–8838 (2020).
67. Cai, X. et al. An intrinsically disordered antimicrobial peptide dendrimer from stereorandomized virtual screening. *Cell Rep. Phys. Sci.* **3**, 101161 (2022).
68. Performance standards for antimicrobial susceptibility testing. Accessed 30 April 2025. https://cdn.bfldr.com/YLD4EVFU/at/hvshwc8rxbsbnnmtqp9f3886/m100ed35e_sample.pdf.
69. Stach, M. et al. Membrane disrupting antimicrobial peptide dendrimers with multiple amino termini. *Med. Chem. Commun.* **3**, 86–89 (2012).
70. Twentyman, P. & Luscombe, M. A study of some variables in a tetrazolium dye (MTT) based assay for cell growth and chemosensitivity. *Br. J. Cancer* **56**, 279–285 (1987).
71. Wenzel, M. et al. The multifaceted antibacterial mechanisms of the pioneering peptide antibiotics Tyrocidine and Gramicidin S. *mBio* **9**, e00802-18 (2018).
72. Schindelin, J. et al. Fiji: an open-source platform for biological-image analysis. *Nat. Anal. Methods* **9**, 676–682 (2012).
73. Ducret, A., Quardokus, E. M. & Brun, Y. V. MicrobeJ, a tool for high throughput bacterial cell detection and quantitative analysis. *Nat. Microbiol.* **1**, 16077 (2016).
74. Syvertsson, S., Vischer, N. O. E., Gao, Y. & Hamoen, L. W. When phase contrast fails: ChainTracer and NucTracer, two ImageJ methods for semi-automated single cell analysis using membrane or DNA staining. *PLoS One* **11**, e0151267 (2016).
75. Wei, Q. et al. Imaging and sizing of single DNA molecules on a mobile phone. *ACS Nano* **8**, 12725–12733 (2014).
76. Rosenblatt, J., Vargas-Cruz, N., Reitzel, R. & Raad, I. Assessment of the potential for inducing resistance in multidrug-resistant organisms from exposure to Minocycline, Rifampin, and Chlorhexidine used to treat intravascular devices. *Antimicrob. Agents Chemother.* **63**, 9 (2019).
77. Kugelberg, E. et al. Establishment of a superficial skin infection model in mice by using staphylococcus aureus and streptococcus pyogenes. *Antimicrob. Agents Chemother.* **49**, 3435–3441 (2005).

Acknowledgements

We sincerely thank Prof. Jean-Louis Reymond for hosting and supporting our research group. Prof. Christoph von Ballmoos and Dr. Nicolas Dolder are acknowledged for giving the opportunity to use their microscope facility. Nicola Christian Lüdi is acknowledged for ICP-MS measurements. A.F. and C.O. gratefully acknowledge funding from the Swiss National Science Foundation Ambizione grant PZ00P2_202016 and from a Research Partnership Grant and support by the University of Bern. M.W. received funding from Chalmers University of Technology. R.R. and O.A.A. were supported by the Wenner Gren Foundations (UPD-2021-0186 and UPD-2021-0036). AA and DS thank UGC, India whereas RM thanks DST-INSPIRE for their fellowship. Parts of the project were conducted during a study visit funded by the National Doctoral Programme in Infection and Antibiotics (NDPIA, to ABS) and a study visit of C.O. to Sweden was kindly funded by University of Bern.

Author contributions

Conceptualization: Ç.Ö., A.B.S., S.C., M.W., and A.F. Data Curation: Ç.Ö., A.B.S., R.R., O.A.A., S.C., M.W., and A.F. Formal Analysis: Ç.Ö., A.B.S., R.R., and O.A.A. Funding Acquisition: A.B.S., F.W., M.W., and A.F. Investigation: Ç.Ö., A.A., R.M., D.S., A.B.S., R.R., and O.A.A. Methodology: Ç.Ö., A.A., R.M., D.S., A.B.S., F.W., and M.W. Project Administration: F.W., M.W., and A.F. Resources: F.W., S.C., M.W., and A.F. Supervision: A.B.S., O.A.A., F.W., S.C., M.W., and A.F. Validation: Ç.Ö., A.B.S., and O.A.A. Visualization: Ç.Ö., A.A., R.M., D.S., A.B.S., S.C., and A.F. Writing—Original Draft Preparation: Ç.Ö., A.B.S., M.W., and A.F. Writing—Review & Editing: Ç.Ö., A.B.S., R.R., O.A.A., F.W., S.C., M.W., and A.F.

Competing interests

The authors declare no competing interests.

Additional information

Supplementary information The online version contains supplementary material available at https://doi.org/10.1038/s44259-026-00211-w.

Correspondence and requests for materials should be addressed to Michaela Wenzel or Angelo Frei.